Biomedical Physics & Engineering Express

ENDORSED BY IPEM Institute of Physics and Engineering in Medicine

PAPER • OPEN ACCESS

Colorectal tumor 3D *in vitro* models: advantages of biofabrication for the recapitulation of early stages of tumour development

To cite this article: J M Rios de la Rosa *et al* 2018 *Biomed. Phys. Eng. Express* **4** 045010

Biomedical Physics & Engineering Express

PAPER

Colorectal tumor 3D *in vitro* models: advantages of biofabrication for the recapitulation of early stages of tumour development

J M Rios de la Rosa[1,2], **J Wubetu**[1], **N Tirelli**[1,3] **and A Tirella**[1,2]

[1] Division of Pharmacy and Optometry, Faculty of Biology, Medicine and Health, University of Manchester, Manchester Academic Health Science Centre, Oxford Road, Manchester, M13 9PL, United Kingdom
[2] NorthWest Centre for Advanced Drug Delivery (NoWCADD), Faculty of Biology, Medicine and Health, University of Manchester, Oxford Road, Manchester, M13 9PT, United Kingdom
[3] Laboratory of Polymers and Biomaterials, Fondazione Istituto Italiano di Tecnologia, 16163 Genova, Italy

E-mail: annalisa.tirella@manchester.ac.uk

Keywords: 3D *in vitro* model, colorectal cancer, biofabrication, CD44, alginate hydrogel, spheroids

OPEN ACCESS

RECEIVED
21 March 2018

REVISED
11 April 2018

ACCEPTED FOR PUBLICATION
2 May 2018

PUBLISHED
17 May 2018

Abstract

The majority of cancer-related *in vitro* studies are conducted on cell monolayers or spheroids. Although this approach has led to key discoveries, it still has a poor outcome in recapitulating the different stages of tumor development. The advent of novel three-dimensional (3D) systems and technological methods for their fabrication is set to improve the field, offering a more physiologically relevant and high throughput *in vitro* system for the study of tumor development and treatment. Here we describe the fabrication of alginate-based 3D models that recapitulate the early stages of colorectal cancer, tracking two of the main biomarkers for tumor development: CD44 and HIF-1α. We optimized the fabrication process to obtain alginate micro-beads with controlled size and stiffness, mimicking the early stages of colorectal cancer. Human colorectal HCT-116 cancer cells were encapsulated with controlled initial number, and cell viability and protein expression of said 3D *in vitro* models was compared to that of current gold standards (cell monolayers and spheroids). Our results evidenced that encapsulated HCT-116 demonstrated a high viability, increase in stem-like cell populations (increased expression of CD44) and reduced hypoxic regions (lower HIF-1a expression) compared to spheroid cultures. In conclusion we show that our biofabricated system is a highly reproducible and easily accessible alternative to study cell behavior, allowing to better mimic the early stages of colorectal cancer in comparison to other *in vitro* models. The use of biofabricated *in vitro* models will improve the translatability of results, in particular when testing strategies for therapeutic intervention.

1. Introduction

Colorectal cancer (CRC), a form of cancer that originates from the large bowel or rectum, is the third most commonly diagnosed malignancy and a major cause of cancer-related mortality in the Western world [1]. In spite of the relatively high survival rates at early stages of the disease, spreading of CRC to other parts of the body, in particular to the liver, results in hard-to-treat conditions that generally have a poor outlook (14% 5-year relative survival rate for stage IV CRC, according to SEER Research Data 2007–2014 [2]). Novel and simple models of CRC initiation, maintenance and invasive processes are therefore required to assist the understanding of the disease and the design and testing of new therapies that effectively block tumor progression, ultimately leading to an overall increase in patient survival rates.

CRC has been associated with chronic inflammation and, increasingly, with atypical inflammatory responses, as discussed in a complete review by Lasry *et al* [3]. Inflammatory processes are known to be triggered from the earliest stages of tumor onset, directly impacting on tumor development and progression. Since the early 20th century, tumors have been described as 'the wound that will not heal' [4]: the setup of the tumor microenvironment (TME) and its remodeling are operated by recruitment of tumor-associated macrophages and cancer-associated fibroblasts, whose function is orchestrated by cancer cells to promote

invasion and colonization of distal tissues [5]. One of the main issues of current pre-clinical *in vitro* models for the study of CRC is the use of standard polystyrene plates (TCP, tissue cell plate) as cell culture substrates. In these traditional models, cells (typically immortalized cell lines) are grown as flat monolayers and evaluated for (1) motility/metastatic potential, (2) expression of relevant biomarkers, and (3) drug efficacy/resistance. More relevant *in vitro* models have been proposed with the inclusion of a second cell type, i.e. co-culture, to understand the crosstalk between cancer and stromal inflammatory cells in the tumor microenvironment (TME). However, the complexity of tumor initiation and progression is difficult to recapitulate in such bi-dimensional (2D) systems; as already demonstrated over the last decade, this strategy leads to a very poor rate of success in terms of *in vivo* translatability of findings [6–8]. In particular, limitations of 2D *in vitro* systems to accurately replicate both cell-cell and cell-matrix interactions in a relevant TME have been widely discussed, highlighting the necessity to include the main components to recapitulate the TME and its development: (a) the spatial configuration, or three-dimensional (3D) cell culture [9–11], (b) the inclusion of supporting materials with mechanical properties similar to those of the extra-cellular matrix (ECM) during disease progression [12–14], and (c) the complexity of *in vivo* signaling and oxygen pressure in the study of cancer development and progression [15]. As a result, there is an urgent need to develop more robust 3D *in vitro* models that closely resemble human cancer tissues, potentially able to integrate multiple cell types in a controlled environment. The generation of multicellular spheroids is the first example of modeling tumors in 3D. The main critique to spheroid cultures is intrinsic to a partial recapitulation of the TME, as spheroids form inner zones containing quiescent and hypoxic cells. In order to mirror the structural architecture of the ECM in 3D, *in vitro* models need to incorporate the knowledge of cancer biology, material science and bioengineering to recreate the most important features *in vitro*: the mechanical and chemical characteristics of the target tissue and the correct transport of nutrients, oxygen, metabolic products, and signaling molecules (figure 1).

Over the last decade, the role of stiffness on cell behavior has been extensively investigated, mainly criticizing the use of standard TCP substrate for 2D culture as it possesses stiffness values (in the order of GPa) not found in the human soft tissues, either healthy or pathological. Rigid culturing substrates are non-representative of such tissues and, together with a geometrically constrained cell growth, they impact on the regulation of cell morphology and signaling cascades involved [16]. In addition, cellular activity products should be also taken into account: 2D *in vitro* systems are simplistic monolayers of live proliferating cells (as dead cells are mostly removed from culture during medium exchange [9]), whereas 3D *in vitro* models are able to closely represent the pathological and heterogeneous confined mix of live cells, dead cells and debris that ultimately influences cancer cells behavior.

Despite all these issues, 2D cultures are still widely used as high throughput models for the identification of tumor-specific markers and for drug screening [17], even though 3D models could in principle predict better tumor cell behavior and help translate the findings to the clinic [18]. The challenge for researchers is to develop simple, reproducible and easily accessible 3D *in vitro* models to translate the vast amount of knowledge established on 2D monolayers over the last 50 years into more physiologically relevant data, with the aim of accelerating findings in pre-clinical research, therapeutic drug screening and early cancer diagnostic. To this end, tissue engineering approaches can be particularly useful, providing fine control over chemical, physical and mechanical properties (as sketched in figure 1). A vast literature has been produced over the last decade, discussing optimal materials, culturing protocols and high-throughput analysis. Among the large number of materials and scaffolds described in literature for the design of such 3D *in vitro* models, alginate hydrogels remain one of the most widely used when it comes to biofabrication of reproducible and robust systems. Alginate is a natural polysaccharide extracted from brown algae, highly biocompatible, biodegradable, non-cytotoxic and extremely bio-inert [19, 20]. Most importantly, alginate is able to rapidly encapsulate living cells with considerably lower stiffness and higher elasticity than those of TCP [21, 22], and its properties can be easily adjusted to biofabrication requirements to obtain 3D constructs with controlled features, e.g. size, shape [23, 24]. Spheroid culture and drug screening studies demonstrated the importance of the third dimension while studying anticancer drug resistance (greater with respect to conventional monolayer cultures). However, there is a need to better model cell-TME interactions to (1) optimize chemotherapeutic candidates, (2) prove their efficacy, and (3) translate findings to the clinic. Shakibaei *et al* [25] firstly evidenced the advantages of using CRC embedded cells in alginate as 3D *in vitro* models for chemotherapeutic testing, reporting on the advantages of using more relevant models to study and prevent drug resistance phenomena.

In this study, we compare the advantages of using biofabrication for cancer research studies, over the gold standard *in vitro* models, TCP monolayer cells and 3D spheroids, respectively. In particular we highlight the urgency to develop early-stage CRC model, as most of the reported studies are more focused on the metastatic processes associated with CRC. Tissue engineered approaches were used to model in 3D the early-stage of CRC via the encapsulation of human epithelial colorectal carcinoma HCT-116 cells in alginate; therefore, no attention was drawn to the vascularization of 3D constructs. Increase in matrix stiffness (about

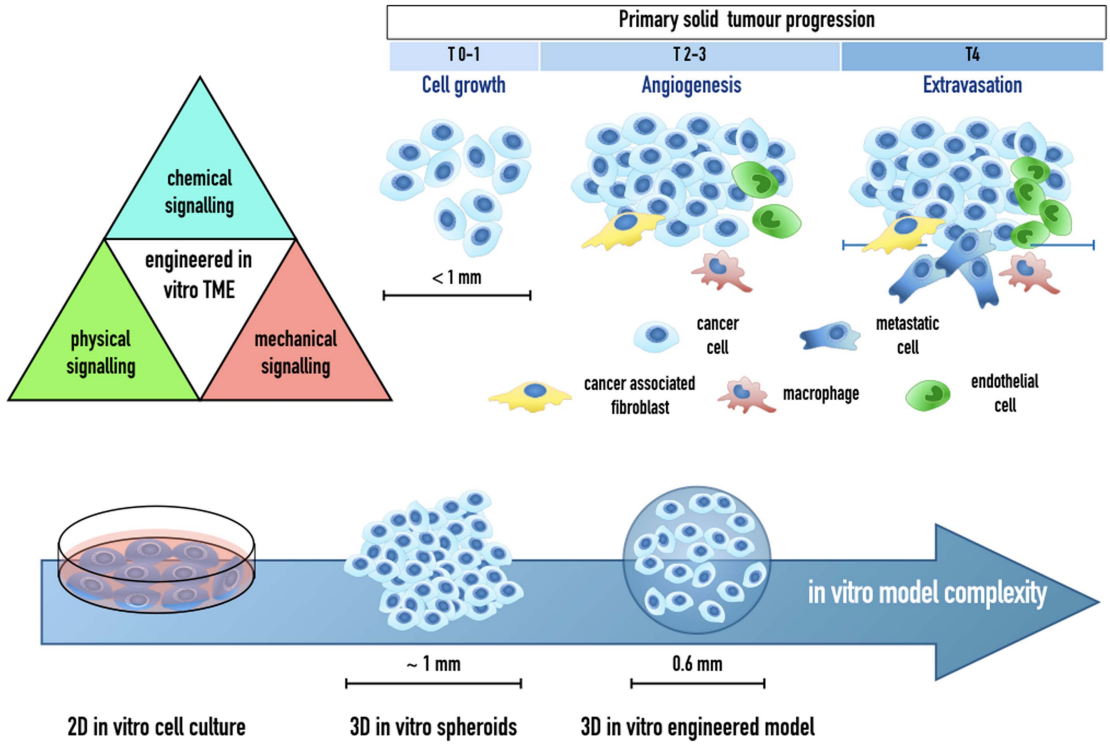

Figure 1. Tissue engineering paradigm applied to cancer: chemical (soluble factors), physical (interstitial pressure, flow materials) and mechanical (stiffness) properties are fundamental design parameters to consider while recapitulating the tumor microenvironment (TME) *in vitro*. These parameters vary as a function of the tumor progression stage, involving different cellular types and promoting cellular polarization towards a motile phenotype, i.e. epithelial-mesenchymal transition (EMT). 3D *in vitro* engineered models provide in principle a more versatile, accessible and high throughput system to speed up the understanding of the disease and the translatability of interventions at the pre-clinical phase.

25 kPa) induces phenotypic variations in HCT-116 toward more aggressive and invasive behavior [24, 26], hence we decided to prepare materials with a stiffness lower than this value (reducing further activation of focal adhesion [27]. We tailored the fabrication process to obtain a 3D *in vitro* model based on the encapsulation of HCT-116 cells in alginate beads, achieving a fine control over bead size and initial cell number. This helped us to match the mechanical and oxygen provision requirements, adjusting alginate concentration (2% w/v), fabrication parameters (voltage, flow rate, frequency), calcium chloride concentration (500 mM) and gelling time (5 min) to obtain microspheres with a diameter smaller than 600 μm (critical thickness for oxygen diffusion in hydrogels [28–30]) and with a final stiffness of approximately 10–15 kPa [31–33]. Moreover, cell number was selected avoiding high density values, typical of late stages of tumor progression, with more invasive cell behavior. We compared the performance of biofabricated 3D models against that of the gold standard currently used in cancer research, i.e. TCP (2D) and spheroids (3D), focusing on cell growth and expression of CD44 (as a marker of stem-like cell population, tumor progression and metastatic potential [34]) and HIF-1α (as a marker of intrinsic hypoxia and tumor progression [15, 35]). We believe that the proposed fabrication method gives rise to *in vitro* models that more closely resemble the physical, mechanical and biochemical characteristics of human colorectal cancer tissue. We believe that our 3D CRC *in vitro* model is a suitable, simple, highly reproducible and easily accessible system to study cancer biology and tumor cell behavior from the early stages of tumor progression. The novelty of this approach will enable to identify and understand the role of key factors driving tumor growth and invasion; this simple, robust and highly reproducible biofabricated 3D *in vitro* model will be a starting point for further studies including pre-clinical models of other cancer types, with the ultimate goal of speeding up drug screening and identifying drug resistance mechanisms at distinctive stages of tumor development.

2. Materials and methods

2.1. Alginate beads preparation

2.1.1. Materials

Alginic acid sodium salt from brown algae (Mw 120 000–190 000 g/moL, 1.56 M/G ratio, Cat.no. A0682, Sigma Aldrich, UK) was dissolved at a concentration of 2% (w/v) in HEPES buffered saline (HBS) consisting of 150 mM NaCl AR grade (433209, Sigma-Aldrich, UK) and 20 mM HEPES (H4034, Sigma Aldrich UK). The solution was mechanically stirred until complete solubilization of alginate (1000 rpm,

30 °C, 2 h). Alginate solution was finally sterile filtered using 0.22 μm PES filter (SLGP033RS, Merck, UK). A 500 mM calcium chloride solution (HEPES) (C1016, Sigma Aldrich, UK) was prepared and sterile filtered prior use (0.22 μm PES filter, SLGP033RS, Merck, UK).

2.1.2. Micro-bead preparation

In this study, an Inotech encapsulator (IE-50, Serial No. 05.002.01–2005, Inotech) was equipped with a nozzle with internal diameter of 300 μm. Briefly, a disposable syringe was filled with 2% (w/v) alginate solution in HBS, and alginate droplets were collected and physically gelled in 500 mM calcium chloride, gently stirred (100 rpm) to avoid bead aggregation during the gelation step. To standardize the fabrication procedure, 1 ml of alginate solution was ejected and the formed beads were kept in the gelation bath for 5 min at room temperature. After this time, alginate beads were collected using sterile 15 mm Netwell™ inserts with 74 μm mesh size polyester membrane (#3477, Constar, USA), rinsed with distilled water and then collected in distilled water to a final 2 ml volume. During the optimization of micro-beads fabrication, (1) alginate solution flow rate, (2) vibration of the extrusion head (frequency and amplitude) and (3) voltage of the electric field were varied to obtain spherical beads with diameter smaller than 600 μm in diameter.

2.2. Cell culture

The human colorectal cancer cell line HCT-116 (CCL-247™) was purchased from ATCC (USA) and cultured in DMEM/F-12 medium (D6546), supplemented with 10% (v/v) fetal bovine serum (FBS, F7524) and 1% (v/v) penicillin/streptomycin (P4333), in a humidified 5% (v/v) CO_2 air atmosphere at 37 °C. Please note that all materials were purchased from Sigma-Aldrich (UK), unless specified otherwise. Cells were maintained at less than 80% confluency and discarded upon reaching passage number 25.

2.2.1. 3D in vitro *model: alginate beads*

HCT-116 cells were suspended in a 2% (w/v) alginate solution in HBS. Briefly, cells were detached with Trypsin-EDTA 0.25% (T4049, Sigma-Aldrich, UK) once 70%–80% confluency was reached, centrifuged and re-suspended in supplemented DMEM/F-12. Aliquots of 1×10^6, 2×10^6 and 5×10^6 cells were centrifuged and gently suspended in 1 ml of 2% (w/v) alginate solution, obtaining a final HCT-116 suspension in alginate of 1×10^6 cells ml^{-1}, 2×10^6 cells ml^{-1} and 5×10^6 cells ml^{-1}, respectively. Cell suspensions in alginate were pipetted in a sterile disposable syringe and mounted on the syringe driver of the Encapsulator system, placed in a Category II Safety Cabinet. Optimized fabrication settings were used to fabricate the 3D *in vitro* models (flow rate = 8.9 ml min^{-1}, frequency = 5500 Hz, Voltage = 1 kV), beads encapsulating HCT-116 were dropped and gelled for 5 min in a calcium chloride solution and finally collected as previously described. After collection, beads were transferred into 12-well plates with complete DMEM/F-12 cell culture medium and cultured in humidified 5% (v/v) CO_2 air atmosphere at 37 °C up to 5 days. Please note that all parts of the Encapsulator system were sterilized with 70% (v/v) Ethanol solution in water and exposed to UV radiation for 30 min prior to use.

2.2.2. 3D in vitro *model: spheroids*

HCT-116 cells (1000 cells/well) were seeded into 96-well Ultra Low Attachment Corning® Spheroid Microplates (#4515) in supplemented DMEM/F-12 and cultured in humidified 5% (v/v) CO_2 air atmosphere at 37 °C.

2.2.3. 2D in vitro *model: conventional tissue-culture plastic (TCP) cell monolayers*

HCT-116 cells were seeded at a density of 0.5×10^4 cells cm^{-2} in polystyrene 12-well plates with flat bottom (#3513, Corning, UK), with approximately 1.9×10^4 HCT-116 cells per well. To evaluate the effect of alginate on cultured cells, HCT-116 suspended in a 2% (w/v) alginate solution were used as a control.

2.3. Alginate micro-beads

2.3.1. Size characterization

Alginate beads were characterized in size and shape first as a function of the different fabrication parameters, then as function of the number of encapsulated cells. Phase contrast images of fabricated beads were acquired using an inverted microscope (DMI6000B, Leica microsystems, UK) coupled with a 5.5 Neo sCMOS camera (Andor, UK). The μManager software (v.1.46, Vale Lab, UCSF, USA) was used to control both microscope and camera, as well as to capture images. For acquisitions a dry 2.5× and a dry 10× objectives were used. Images were processed and analyzed using ImageJ software (v1.49p, http://rsb.info.nih.gov/ij). Note that a minimum number of 50 beads for each experiment (with n = 3 technical replicates) were imaged and measured to ensure statistical validity.

2.3.2. Bead dissolution

To gently dissolve alginate micro-beads and recover viable encapsulated HCT-116 cells, the following method was used. A calcium-sequestering solution was prepared dissolving HEPES (H4034, Sigma Aldrich, UK) and trisodium citrate dihydrate (W302600-K, Sigma Aldrich, UK) in phosphate buffered saline (PBS, D1408, Sigma Aldrich, UK) to a final concentration of 100 mM and 500 mM, respectively. The pH was adjusted to 7.3 by addition of 1 M NaOH

(aq.) (J/7620/15, Thermo Fisher Scientific, UK) to ensure a physiological pH value during beads disruption. Prior to use, the disrupting solution was sterile-filtered (0.22 μm PES filter, SLGP033RS, Merck, UK), then micro-beads were washed with PBS (n = 2, room temperature), 2 ml of bead-disrupting solution were added to each well (containing an average number of 30 000 beads) and incubated for 10 min at 37 °C, 5% (v/v) CO_2. Finally, to ensure complete alginate micro-bead disruption and cell re-suspension, an additional gently pipetting step was performed and a final average number of 37 000 cells were recovered.

2.4. Cell viability and growth

2.4.1. Live/dead assay: flow cytometry

Flow cytometry acquisitions were performed after staining with Live/Dead kit (L3224, Thermo Fisher Scientific, UK). Briefly, HCT-116 cells were encapsulated in alginate beads, plated in 12-well plates and cultured in standard conditions (time point = 5 days, n = 3). As a control, HCT-116 cells were plated in a 12-well plate (0.5×10^4 cells cm^{-2}) and cultured with or without alginate. At each time point, 2D controls were washed with PBS, detached with Trypsin-EDTA (5 min, 37 °C), and then cell suspensions were transferred to 1.5 ml vials. For the 3D systems, beads were washed with PBS at each time point, 1 ml of dissolution buffer was added to each well and after incubation (10 min at 37 °C) cell suspensions were transferred to 1.5 ml vials. After centrifugation (1000 rpm, 5 min, room temperature), 50 μl of staining solution (prepared following manufacturer's instructions) and 50 μl of PBS were added to each vial, cells were gently re-suspended and incubated for 15 min at room temperature. Two washing steps with PBS were performed (1000 rpm, 5 min, room temperature) and finally cells were gently re-suspended in PBS and stored on ice prior to flow cytometry measurements. Live/Dead counting was measured via flow cytometry (BD LSRFortessa cell analyser/flow cytometer) detecting live (calcein-AM, 494/517 nm) and dead (ethidium homodimer-1, 517/617 nm) cells on 5000 individual events.

2.4.2. Live/dead assay: imaging

HCT-116 cells encapsulated in alginate beads were additionally imaged after staining with Live/Dead kit at different time points (24, 48 and 72 h). Briefly, HCT-116 were encapsulated in alginate beads, plated in 12-well plates and cultured in standard conditions. At each time point, beads were washed with PBS, transferred to a 96-well plate, and finally 50 μl of staining solution (prepared following manufacturer's instructions) and 50 μl of PBS were added to each well. Encapsulated cells were incubated with (15 min, room temperature). Finally, two washing steps with PBS were performed and bead images were acquired using a fluorescent inverted microscope inverted microscope (Leica DMI6000B, Leica Microsystems, UK) coupled with a 5.5 Neo sCMOS camera (Andor, UK). The μManager software (v.1.46, Vale Lab, UCSF, USA) was used to control both microscope and camera, as well as to capture images. For acquisitions, a dry 10× objective (N Plan 10x/0.25 PH1, Leica) with filter cubes I3 (BP 450-490, LP 515) and N2.1 (BP 515-560, LP 590) was used. Z-stack were acquired every 50 μm. Images were processed using ImageJ v1.49p.

2.4.3. Trypan blue

Viability of encapsulated HCT-116 cells was measured at different time points and results were compared with the 2D controls. Trypan blue was used as qualitative and simple method to monitor cell viability over time i.e. 24, 48 and 72 h after beads fabrication. For the 3D system, beads were plated in 12-well plates and cultured in standard conditions as previously described. In the case of 2D controls, cells were washed with PBS, detached with trypsin-EDTA solution (5 min, 37 °C), and transferred to vials. Cell suspensions were centrifuged (1000 rpm, 5 min, room temperature) and cell pellets were gently suspended in 900 μl PBS and 100 μl of 0.4% (w/v) Trypan Blue were added to each vial. Finally, 10 μl of cell suspension were gently pipetted in a hemocytometer for live/dead exclusion counting using an inverted light microscope (Olympus CKX41). An average live/ dead count and percentage was obtained at each time point (n = 4). Growth rates of cells in alginate micro-beads (about 30 000 beads in each 12-well plate, n = 4 for each time point) was compared with that of the standard TCP (initial seeding density of 2×10^4 cells cm^{-2}, n = 4 for each time point) and spheroid (initial seeding density of 3×10^3 cells cm^{-2}, n = 3 for each time point) controls, measuring the number of viable cells at different time points. Alginate micro-beads were disrupted and cells on TCP and spheroids trypsinized following the same procedures described above. Collected cells were centrifuged (1000 rpm, 5 min, room temperature) and gently suspended in 900 μl PBS, followed by addition of 100 μl 0.4% (w/v) Trypan Blue (aq.) solution. Finally, 10 μl of cell suspension was pipetted in a hemocytometer for live/dead exclusion counting using an inverted light microscope (Olympus CKX41). Cell number was averaged across technical replicates (n = 3) and biological replicates (at least n = 3) for each time point.

2.5. Tumor progression biomarkers: CD44 and HIF-1α

HCT-116 cells were cultured in 2D and 3D *in vitro* models (as previously described) and the expression of CD44 (total, spanning both standard and variant isoforms of the protein) and HIF-1α measured over time, i.e. 3 and 5 days. Controls (2D, TCP) were washed with PBS, cells were detached using Trypsin-EDTA 0.25%, centrifuged (1000 rpm, 5 min) and

suspended in FACS Buffer (phosphate buffer solution supplemented with 5% FBS and 0.1% w/v sodium azide). Alginate micro-beads (3D) were first washed with HBS, then disrupted by adding 2 ml of dissolution buffer as previously described, and finally cell suspensions were transferred into 2 ml vials and centrifuged at 1000 rpm for 5 min HCT-116 spheroids (3D) were collected and disaggregated into suspensions of individually dispersed cell by incubation with Trypsin-EDTA 0.25% for 15 min at 37 °C. Cells were then centrifuged at 1000 rpm for 5 min Approximately 500 000 cells were collected for each culturing method, and stained first with 100 μl of rat anti-human CD44: AF647 (1:400, 0.125 μg of antibody to stain 0.5 $\times$ 10^6 cells in a volume of 100 μl) (Clone IM7, BioLegend), then fixed with 0.4% PFA for 15 min at room temperature, permeabilized with 0.25% Triton-X (in PBS BSA 0.1%) for 15 min at room temperature, and finally stained with 100 μl of mouse anti-human HIF-1α:PE (1:40, 0.0625 μg of antibody to stain 0.5 $\times$ 10^6 cells in a volume of 100 μl) (Clone 546-16, BioLegend) in FACS buffer for 30 min at room temperature. To remove any excess of unbound antibody, two serial steps of washing/centrifugation with PBS were performed. Finally, samples were suspended in 400 μl of PBS, prior to flow cytometry measurements. The expression of the two markers was detected on at least 2000 live and individual cells using a BD LSRFortessa cytometer (BD Bioscience, San Jose CA, USA) equipped with the FACSDiva software (v8.0.1). Data were analyzed with FlowJo (vX.0.7, Tree Star, Ashland, OR, USA) after gating live cells in the FSC/SSC window and singlets in the FSC- H/FSC-A window, respectively. The MFI of the isotype control was used as threshold to calculate the MFI of the marker of interest.

2.6. Statistical analysis

Data were analyzed via GraphPad Prism 7 software (GraphPad Software, Inc., San Diego, CA, USA). Two-way ANOVA was used to compare biomarker expression. Differences between groups were considered significant with a P value <0.05.

3. Results

3.1. Alginate bead fabrication and characterization

The Inotech IE-50 is a flexible microencapsulation system that allows a controlled and automated bead fabrication process. Fabrication process can be tailored by varying the nozzle diameter, the viscosity of the solution, and other additional controlled parameters in order to produce uniform spherical beads with a controlled size. The parameters controlled in this study were: alginate solution flow rate, vibration of the extrusion head (frequency and amplitude), and voltage of the electric field (effect shown in figure 2(a)). During the first optimization process, a 2% (w/v) alginate solution in HBS (aq.) was used to fabricate alginate beads. At this stage, alginate beads were imaged using a light microscope and classified in size and shape for each set of fabrication parameters (tables 1–3). The optimal set of parameters to obtain spherical and uniform alginate beads with a diameter of 540 $\pm$ 20 μm beads were selected as follows: 300 μm nozzle, 5.5 kHz Frequency, 1 kV Voltage, and 8.9 ml min^{-1} flow rate.

3.2. Encapsulation of HCT-116 cells

To identify the optimal bead composition that fostered cell viability over 5 days of cell culture, different HCT-116 cell densities suspended in 2% (w/v) alginate in HBS were tested, i.e. 1, 3 and 5 $\times$ 10^6 cells ml^{-1}. Alginate beads encapsulating HCT-116 at different cell densities were also analyzed in terms of size and shape, after fabrication and during cell culture. A cell density of 1 $\times$ 10^6 cells ml^{-1} was found to be optimal to fabricate cell-loaded beads with similar characteristics to their empty counterpart, i.e. spherical and homogeneous beads with a diameter of 540 $\pm$ 20 μm (figures 2(b) and (c)). Higher cell densities produced non-spherical and considerably larger beads, with significant cell outgrowth (figure 2(e)).

3.3. Cell viability and growth: 2D versus 3D

Beads fabricated using the optimized parameters (figure 2(d), detailed in figure 3(a)) were finally tested, assessing for differences in cell behavior between 2D and 3D *in vitro* models. Fluorescence microscopy and flow cytometry data of Live/Dead staining did not reveal areas of pronounced cell death caused by the fabrication procedure or hypoxic regions of cells encapsulated within alginate beads (figures 4(a), (b)). We observed an increase of dead cells in spheroid cultures, most likely as a result of the formation of a necrotic core. Cell viability was additionally measured using conventional Trypan blue staining (hemocytometer count) following beads dissolution and cell recovery or spheroids disruption for 3D models. Hemocytometer counts revealed an average cell viability of 60% for encapsulated cells in 3D models compared to 2D controls 24 h after encapsulation (data not shown). Trypan blue staining and hemocytometer counting were additionally used to obtain the growing curve in different culture conditions up to 72 h. As shown in figure 3(d), the growth rates of HCT-116 cells cultured either in 2D or encapsulated in alginate (3D) were indistinguishable, and as expected, the presence of alginate did not have an impact on cell proliferation . On the other hand, HCT-116 in spheroids culture exhibit a different growth profile: with slow growth rate when they are forming cell-cell junction (up to 48 h) and higher growth rate when the spheroid is formed and cancer cells start to exponentially growth mimicking tumor progression (72 h, as reported in the literature).

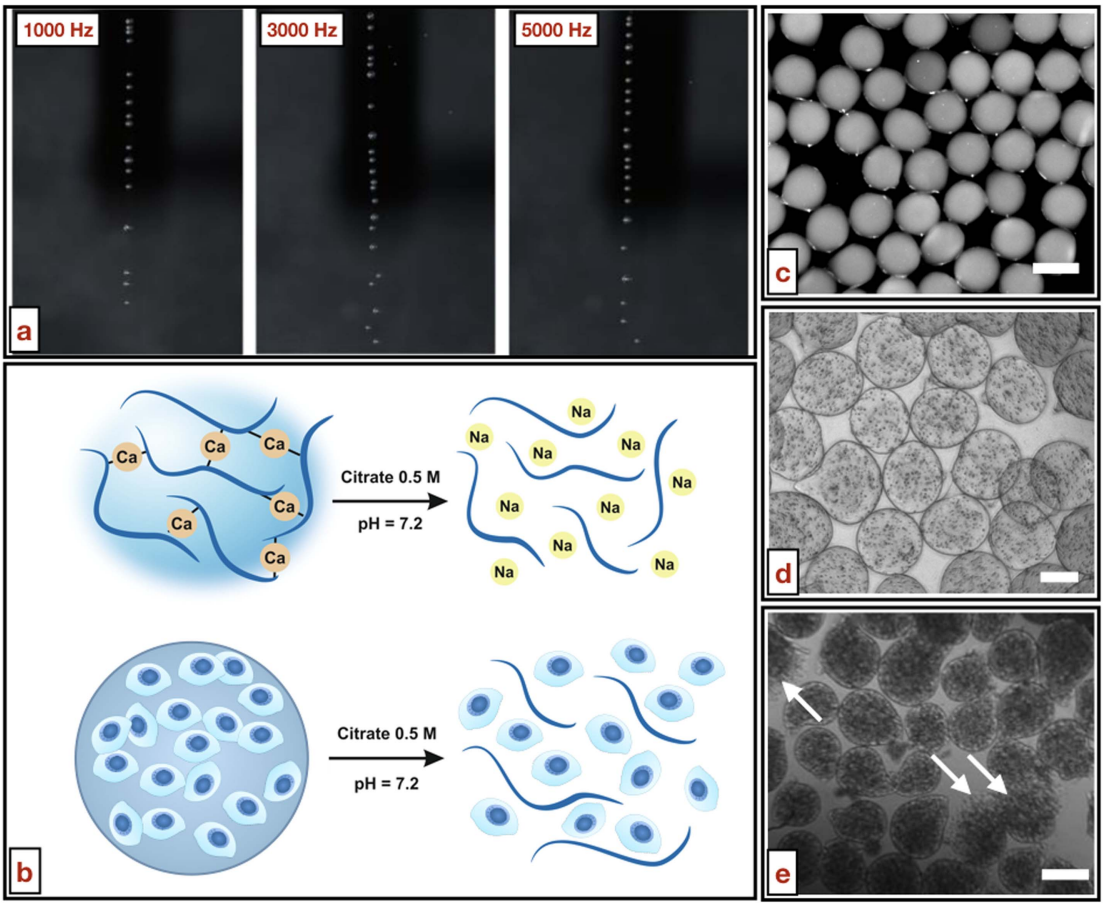

Figure 2. Alginate bead fabrication using a 2% (w/v) alginate in HBS; fabrication parameters: flow rate 8.9 l min^{-1}, frequency 5500 Hz, Voltage 1 kV. (a) Influence of fabricating parameters: example of vibrational head frequency in disruption of alginate stream. Please note that with increasing frequency the stream is more homogenously disrupted, returning beads with mono-dispersed size. (b) Sketch of bead dissolution, allowing easy downstream analysis on cultured cells. (c) Example of empty alginate beads obtained after optimization of the fabrication process (size of 540 $\pm$ 20 μm, scale bar 600 μm). (d) Example of HCT-116 cells encapsulated in alginate beads (initial cell density of 1 $\times$ 10^6 cells ml^{-1}, scale bar 300 μm). (e) Example of HCT-116 cells encapsulated in alginate beads (initial cell density of 5 $\times$ 10^6 cells ml^{-1}, scale bar 600 μm). Alginate beads obtained with higher cell density were slightly bigger (average diameter of 610 $\pm$ 15 μm) and presented deformities due to high cell densities (highlighted with arrows).

Table 1. Average bead diameters with varying flow rate. Diameter is shown as average $\pm$ st.dev. measured (n = 3 technical replicates).

			Flow rate		
Alginate concentration	Frequency (kHz)	Voltage (kV)	Encapsulator setting	Equivalent ml min^{-1}	Average diameter $\pm$ SD (μm)
2% (w/v)	2.5	1.0	700	7.3	619.0 $\pm$ 28.5
			750	7.8	593.0 $\pm$ 46.5
			800	8.4	537.5 $\pm$ 42.5
			850	8.9	504.5 $\pm$ 25.0
			900	9.4	518.5 $\pm$ 37.0
			950	9.9	666.0 $\pm$ 43.0

Table 2. Average bead diameters with varying voltage. Diameter is shown as average $\pm$ st.dev. measured (n = 3 technical replicates).

			Flow rate		
Alginate concentration	Frequency (kHz)	Voltage (kV)	Encapsulator setting	Equivalent ml min^{-1}	Average diameter $\pm$ SD (μm)
2% (w/v)	0.5	0.6	850	8.9	574.5 $\pm$ 35.0
		1.0			586.5 $\pm$ 22.0
		1.2			577.5 $\pm$ 22.5
		1.6			584.0 $\pm$ 267.0

Table 3. Average bead diameters with varying frequency. Diameter is shown as average ± st.dev. measured (n = 3 technical replicates).

Alginate concentration	Frequency (kHz)	Voltage (kV)	Flow rate		Average diameter ± SD (μm)
			Encapsulator setting	Equivalent ml min^{-1}	
2% (w/v)	1.0	1.0	850	8.9	586.0 ± 26.0
	1.5				594.0 ± 19.0
	2.0				603.5 ± 28.5
	2.5				615.0 ± 27.5
	3.0				611.0 ± 23.5
	3.5				612.0 ± 24.5
	4.0				595.0 ± 22.5
	4.5				598.0 ± 27.0
	5.0				593.0 ± 28.0

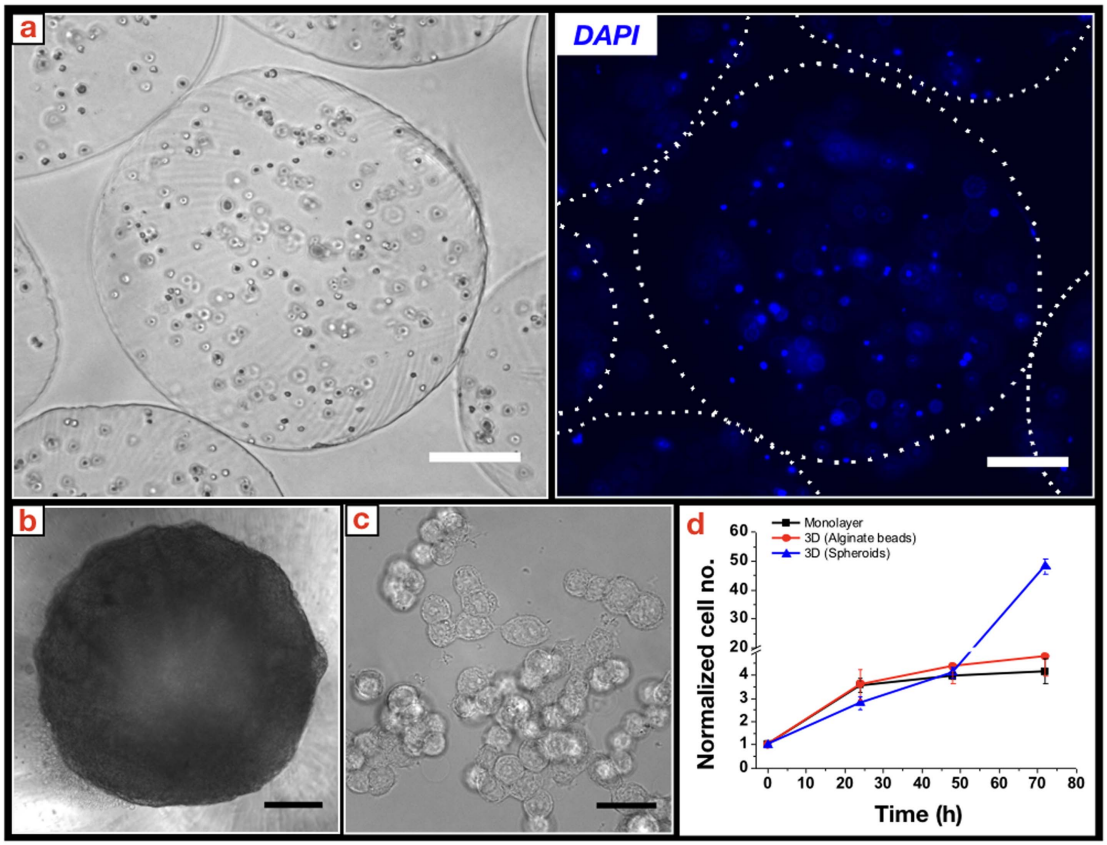

Figure 3. Comparison between *in vitro* models: cell growth. (a) *Left:* Detailed bright-field image of alginate beads encapsulating 1×10^6 HCT-116 cells ml^{-1} after 3 days of culture (average bead size of 540 μm; fabrication parameters: flow rate 8.9 ml min^{-1}, frequency 5500 Hz, Voltage 1 kV) (scale bar 200 μm). *Right:* Fluorescence image (DAPI/nuclei, beads evidenced in the figure with a dotted line). (b) Bright-field image of a representative HCT-116 spheroid after 3 days of culture in Ultra-Low Attachment surface 96-well plates (initial seeding density 1000 cells/well) (scale bar 250 μm). (c) Bright-field image of HCT-116 cells grown as a conventional monolayer (scale bar 50 μm). (d) Normalized cell number for HCT-116 cells cultured in 2D TPC, 3D alginate beads or 3D spheroids up to 72 h (n = 3, N = 2). Note that a control with HCT-116 cultured on 2D with 2% (w/v) alginate was also tested with no significant variation with respect to the standard 2D control (data not shown).

3.4. CD44 and HIF-1α expression

CD44 variant isoforms (CD44v) are recognized prognostic and diagnostic markers for several tumor types; for instance, CD44v6 has significant prognostic value in CRC and is considered of value in identifying patients with a propensity to develop distant metastasis [36]. In this study we focused our attention on the expression of total CD44 (spanning all variant isoforms) in HCT-116 encapsulated in alginate beads over time and compared this expression with that of the two gold standards currently used in cancer research: 2D TCP and 3D spheroid *in vitro* models. The expression of membrane-anchored CD44 was investigated through direct staining with a fluorescently-labeled antibody and detected via flow cytometry on live cells. We found that CD44 expression was consistently higher in cells grown using 3D models than in those grown as 2D monolayers (figure 4(c)). At

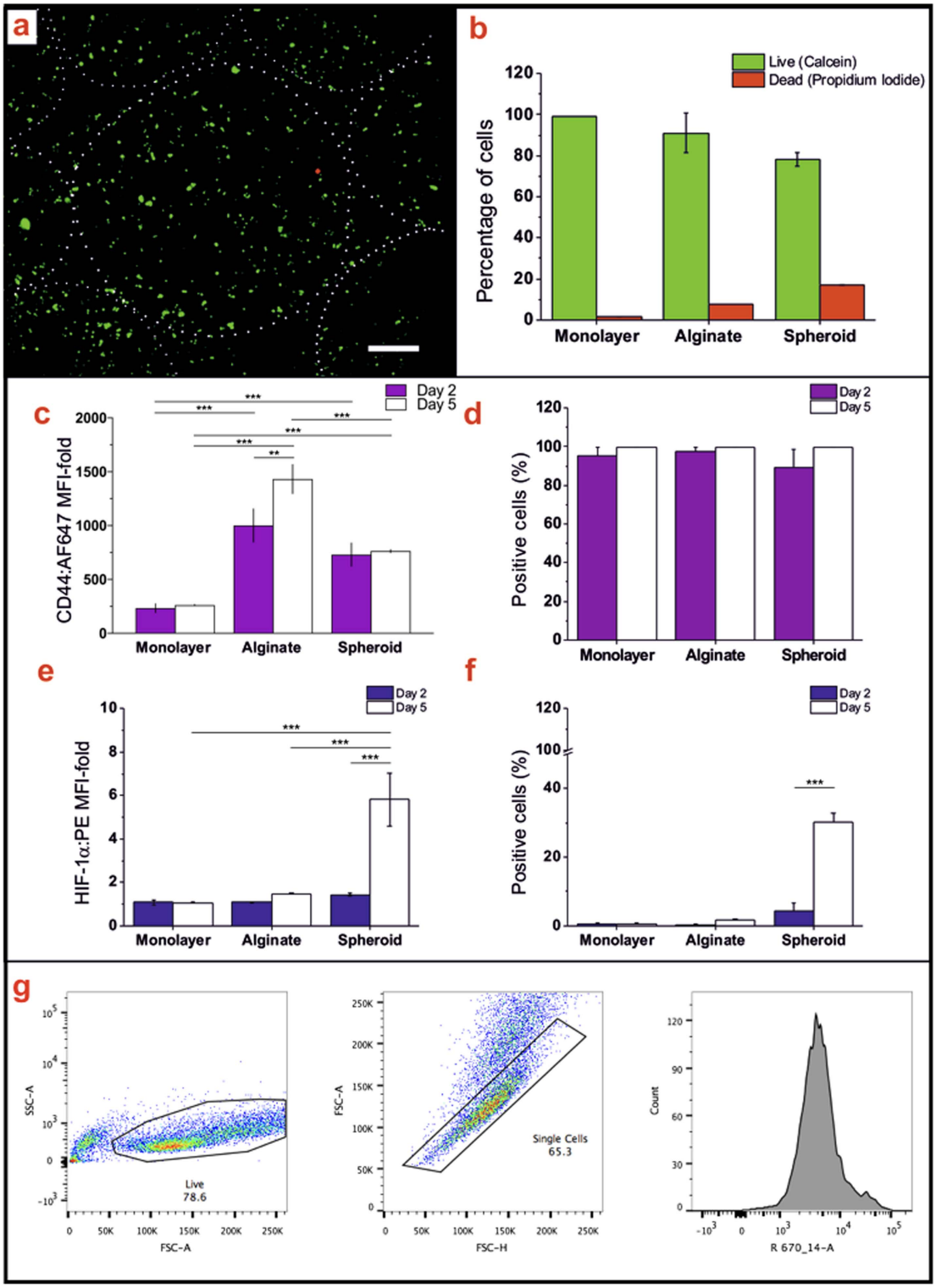

Figure 4. Biological marker comparison in HCT-116 cells cultured as monolayers (2D, TCP) or 3D *in vitro* models (in the form of spheroids or encapsulated in alginate beads) to mimic early stage colorectal cancer. (a) Representative fluorescence microscopy images of HCT-116 encapsulated in alginate beads 24 h after beads fabrication, Live/Dead staining (Live: calcein-AM/green; Dead: propidium iodide/red) (scale bar 200 μm, bead diameter delineated with a dotted line). (b) Live/Dead signal measured with flow cytometry after 5 days of culture (n = 3). Expression of the tumor development-associated markers CD44 (c) and HIF-1α (d) at different time points i.e. 2 or 5 days after seeding/fabrication (n = 3), and respective number of positive cells (e), (f). The statistical analysis refers to the comparison of tumor development-associated markers in distinctive *in vitro* models and different time points: $^{***}P < 0.001$, $^{**}P < 0.01$, $^{*}P < 0.5$ (Two-way ANOVA). (g) Flow cytometry: example of gating strategy used to measure CD44 expression in HCT-116 encapsulated in alginate beads (g): live cells, single cells and histogram.

each time point, all *in vitro* models tested returned more than 95% of positive cells for CD44 (figure 4(d)). Please note that we ruled the influence of alginate on CD44 detection by comparing the 3D models with cells cultured on 2D in the presence of 2% (w/v) alginate (data not reported).

We then focused our attention on HIF-1α, a marker of tumor aggressiveness, invasiveness and resistance to radiotherapy and chemotherapy in a variety of tumors such as cervical [37], triple negative breast [38], and CRC [35]. HIF-1α is a powerful transcription stimulator known to be expressed when the oxygen cannot perfuse into the primary tumor mass, hence generating hypoxic regions that trigger the production of cytoprotective proteins that allow for survival and proliferation. At this stage, cancer cells start to recruit stromal cells involved in angiogenesis. Once the tumor mass reaches the critical dimension of 1–2 mm, it starts to progress to a more invasive and advanced stage [39, 40]. As expected, no HIF-1α protein expression was detected in HCT-116 cultured on TCP. Similar negligible levels of HIF-1α were measured in HCT-116 encapsulated in alginate beads. In contrast, HIF-1α was detected in HCT-116 cultured as spheroids, with significant increase of HIF-1α expression and positive cells over time (figures 4(e), (f)). These results match those seen for HeLa cells, which express HIF-1α when cultured as spheroids both in hypoxia and normoxia [41]. The lack of oxygen and nutrient provision in HCT-116 spheroids is also reflected in the lower cell viability detected for HCT-116 spheroids after 5 days of culture (flow cytometry, figure 4(b)). No significant percentage of dead HCT-116 cells was detected in 3D alginate beads or standard 2D TCP *in vitro* models.

4. Discussion

Over the last decades, significant efforts have been put towards the development of 3D *in vitro* cell models for cancer research studies (e.g. drug discovery and development) due to the disadvantages associated with conventional 2D monolayer culturing, mainly its inability to faithfully recreate the *in vivo* complexity of tumors [42]. The importance of the use of 3D models in both basic research and drug discovery/testing has been extensively discussed [16]. More complex 3D *in vitro* models in cancer research were firstly introduced in form of spheroids [39, 43], showing the advantages of (a) culturing cells in 3D, (b) promoting cell-cell interactions similar to those of the *in vivo* system/animal model, (c) obtaining a heterotypic population closer to the tumor mass, and (d) inducing the formation of a hypoxic core. The latest technological advancement evidenced two main limitation of spheroids: the formation of cell-matrix interaction typical of tumors and the recapitulation of early-stages of tumor progression. More recently, tissue engineering methods were used to develop more sophisticated tumor *in vitro* models able to finely control chemical, physical and mechanical properties, hence recreate in 3D: (a) TME characteristics at different stages of tumor development, (b) cell-cell interactions, and (c) cell-matrix interactions. An example of the advantages in using encapsulated HCT-116 in alginate beads to study CRC chemotherapies and relative drug resistance was reported by Shakibaei *et al* [25], in which effects of potent chemotherapeutics on late and aggressive/metastatic stage of CRC were studied. We here described a novel approach of modelling and biofabricating the early stage of CRC and its TME, allowing a better control over (1) alginate beads dimension and (2) number of CRC cells. Moreover, we compared the CRC stage of HCT-116 cells encapsulated in alginate micro-beads with that of HCT-116 in form of standard spheroids. Our aim was to compare the two 3D *in vitro* models to address the generation of early stage models for CRC, where angiogenesis and stromal response are not yet involved [11, 40, 44, 45]. The first part of the study was dedicated to optimize the fabrication process and obtain beads controlled in size, stiffness and cell number. Then, attention was moved to compare the behavior of encapsulated HCT-116 to cells cultured as spheroids or 2D monolayers in terms of viability and protein expression. During the optimization of the fabrication of alginate-based 3D *in vitro* models, we explored the role of initial cell density as a strategy for the fabrication of early or advanced tumor stages, i.e. lower or higher number of cancerous cells per bead, respectively. However, for this specific study we decided to use a lower cell density (1×10^6 cells ml^{-1}) in order to avoid the need for vascularization required for nourishment [40]. The optimal bead fabrication parameters were then studied. Importantly, the bead diameter was set at values lower than 600 μm so that hypoxic regions (typical of spheroids) could be avoided, which is in turn a key important factor in order to separate the effects of hypoxia and tissue dimensionality in 3D models [46]; and the alginate concentration and gelation ([Ca^{2+}], time) were adjusted so that the final beads had a stiffness of about 10–15 kPa, similar to what reported in literature to preserve a less invasive behavior of HCT-116 cells [26, 31–33, 47].

We observed a different growth rate for spheroids with a peak of cell growth after 72 h of culture, whereas the alginate-beads (3D) and the monolayer (2D) models have a similar growth-rate. Cell viability was not directly affected regardless of the culturing method.

Since 3D *in vitro* models are supposed to be a better alternative for recapitulating tumor progression, we then tried to understand whether cell-cell and cell-material interactions were actually necessary to accurately mimic the TME properties at an early phase of tumor progression. With that aim, we shifted our attention to evaluating the expression of two different biomarkers for tumor progression: CD44 (its overexpression could be indicative of early CRC development and progression [48]) and HIF-1α (its expression could be used as biomarker for CRC tumors in advanced stage [49]). The expression of the two biomarkers was detected at two different time points, i.e. 3 and 5 days, bearing in mind that

uncontrolled cell growth could potentially influence their expression. Remarkably, HCT-116 cells encapsulated in alginate beads expressed higher amounts of total CD44 and lower amounts of HIF-1α compared to cells cultured in the form of spheroids. Therefore, we believe that HCT-116 cells cultured in alginate beads may mimic more accurately the early stages of tumor development ($CD44^{high}/HIF\text{-}1\alpha^{low}$), which would be more difficult to recapitulate in spheroids at relatively short culturing time points (due to low cell number and cell-cell interactions). We believe that the biofabricated 3D *in vitro* model presented in this work offer many advantages for recreating a more physiologically relevant early-stage CRC tumor model in that these hydrogels possess a stiffness similar to that of abdominal soft tissues (as opposed to TCP grown 2D monolayers), and provide an easier platform to investigate colorectal cancer behavior in 3D when compared to spheroids, as our model rules out interference of other factors, such as hypoxia, i.e. it allows to study the effect of dimensionality only.

5. Conclusions

We recreated and validated a biofabrication method to model the early stage colorectal cancer tumor: CRC cells cultured in this novel 3D *in vitro* model were compared with gold standards *in vitro* cell cultures, i.e. monolayer and spheroid. Alginate micro-beads with a known number of encapsulated HCT-116 cells were successfully biofabricated, fostering cell growth and viability, while avoiding hypoxic regions. As cancer progression is spatiotemporally related, hydrogel micro-beads provide a gateway into a 3D cell culture method with high experimental reproducibility and easy access for downstream biological analysis. Despite not fully recreating the complex tumor microenvironment, we have demonstrated that the expression of common cancer markers and drug delivery protein targets, such as CD44, can be mimicked using biofabrication methods. This result may indicate that this model reflects more accurately the expression levels of CD44 linked to tumor onset. Besides, the higher expression of the necrotic factor HIF-1α in spheroids suggests that this 3D model represents more closely the heterogeneous tumor mass that needs of nutrients and oxygen provision, hence vasculature would be necessary in these systems in order to better mimic the pathophysiology of tumor progression.

Our data thus suggest suitability of alginate hydrogels as a platform for 3D cell culture to improve preclinical drug testing in CRC. High throughput 3D *in vitro* systems are certainly the future of cancer research and therapeutics, and we set the first building block for the creation of advanced *in vitro* models of tumor progression. Further investigation on material, vascularization, and integration of stromal cell types will be necessary to recreate the complexity of tumor progression and enhance the outputs of cancer research and drug delivery/testing.

Acknowledgments

Dr Rios de la Rosa is indebted to EPSRC for a PhD studentship (part of the North-West Nanoscience (NoWNano) Doctoral Training Centre, EPSRC grant EP/G03737X/1). Mr Jonathan Wubetu is thankful to MRes Tissue Engineering for Regenerative Medicine (TERM), FMBH, University of Manchester, for supporting this research. The Bioimaging and Flow Cytometry facilities of the Faculty of Life Sciences (University of Manchester) are maintained with grants from BBSRC, Wellcome Trust, and the University of Manchester Strategic Fund. The authors would like to thank Miss Chen Zhao, Miss Bushra Almari, Mr Kajen Suresparan and Miss Alice Spadea for fruitful scientific discussions.

ORCID iDs

A Tirella https://orcid.org/0000-0002-3743-3593

References

[1] Siegel R L, Miller K D and Jemal A 2017 Cancer statistics *CA Cancer J. Clin.* 2017 **67** 7–30
[2] Howlader N *et al* Cancer Statistics Review, 1975-2014 - SEER Statistics, National Cancer Institute. SEER Cancer Statistics Review, 1975-2014. p. (http://seer.cancer.gov/csr/1975_2014/)
[3] Lasry A, Zinger A and Ben-Neriah Y 2016 Inflammatory networks underlying colorectal cancer *Nat. Immunol.* **17** 230–40
[4] Byun J S and Gardner K 2013 Wounds that will not heal: pervasive cellular reprogramming in cancer *American Journal of Pathology. American Society for Investigative Pathology* **182** 1055–64
[5] Hanahan D 2014 Rethinking the war on cancer *Lancet* **383** 558–63
[6] Goodspeed A, Heiser L M, Gray J W and Costello J C 2016 Tumor-derived cell lines as molecular models of cancer pharmacogenomics *Mol. Cancer Res.* **14** 3–13
[7] Katt M E, Placone A L, Wong A D, Xu Z S and Searson P C 2016 *In vitro* tumor models: advantages, disadvantages, variables, and selecting the right platform *Front Bioeng Biotechnol.* **4** 12
[8] Gillet J-P, Varma S and Gottesman M M 2013 The clinical relevance of cancer cell lines *JNCI J. Natl. Cancer Inst.* **105** 452–8
[9] Edmondson R, Broglie J J, Adcock A F and Yang L 2014 Three-dimensional cell culture systems and their applications in drug discovery and cell-based biosensors *Assay Drug Dev. Technol.* **12** 207–18
[10] Fitzgerald K A, Malhotra M, Curtin C M, O'Brien F J and O'Driscoll C M 2015 Life in 3D is never flat: 3D models to optimise drug delivery *J. Control. Release* **215** 39–54
[11] Stock K *et al* 2016 Capturing tumor complexity *in vitro*: Comparative analysis of 2D and 3D tumor models for drug discovery *Sci. Rep.* **6** 28951
[12] Mierke C T 2014 The fundamental role of mechanical properties in the progression of cancer disease and inflammation *Reports Prog. Phys.* **77** 76602
[13] Ehrbar M *et al* 2011 Elucidating the role of matrix stiffness in 3D cell migration and remodeling *Biophys. J.* **100** 284–93

[14] Pathak A and Kumar S 2011 Biophysical regulation of tumor cell invasion: moving beyond matrix stiffness *Integr. Biol. (Camb)* **3** 267–78
[15] Semenza G L 2014 Oxygen sensing, hypoxia-inducible factors, and disease pathophysiology *Annu. Rev. Pathol. Mech. Dis.* **9** 47–71
[16] Smalley K S M and Lioni M 2018 LIFE isn't flat: taking cancer biology to the next dimension *Vitr. Cell Dev. Biol—Animal* **42** 242–7
[17] HogenEsch H and Nikitin A Y 2012 Challenges in pre-clinical testing of anti-cancer drugs in cell culture and in animal models *J. Control. Release* **164** 183–6
[18] Gao S, Shen J, Hornicek F and Duan Z 2017 Three-dimensional (3D) culture in sarcoma research and the clinical significance *Biofabrication* **9** 32003
[19] Ivanovska J *et al* 2016 Biofabrication of 3D alginate-based hydrogel for cancer research: comparison of cell spreading, viability, and adhesion characteristics of colorectal HCT116 tumor cells *Tissue Eng. Part C Methods* **22** 708–15
[20] Lee K Y and Mooney D J 2012 Alginate: properties and biomedical applications *Prog. Polym. Sci.* **37** 106–26
[21] Barralet J E, Wang L, Lawson M, Triffitt J T, Cooper P R and Shelton R M 2005 Comparison of bone marrow cell growth on 2D and 3D alginate hydrogels *J. Mater. Sci., Mater. Med.* **16** 515–9
[22] Braccini I and Pérez S 2001 Molecular basis of Ca2+-induced gelation in alginates and pectins: the egg-box model revisited *Biomacromolecules* **2** 1089–96
[23] Tirella A, Magliaro C, Penta M, Troncone M, Pimentel R and Ahluwalia A 2014 Sphyga: a multiparameter open source tool for fabricating smart and tunable hydrogel microbeads *Biofabrication* **6** 25009
[24] Jabbari E, Sarvestani S K, Daneshian L and Moeinzadeh S 2015 Optimum 3D matrix stiffness for maintenance of cancer stem cells is dependent on tissue origin of cancer cells *PLoS One* **10** e0132377
[25] Shakibaei M, Kraehe P, Popper B, Shayan P, Goel A and Buhrmann C 2015 Curcumin potentiates antitumor activity of 5-fluorouracil in a 3D alginate tumor microenvironment of colorectal cancer *BMC Cancer* **15** 250
[26] Tang X *et al* 2014 A mechanically-induced colon cancer cell population shows increased metastatic potential *Mol. Cancer* **13** 131
[27] Levental K R *et al* 2009 Matrix crosslinking forces tumor progression by enhancing integrin signaling *Cell* **139** 891–906
[28] Amsden B and Turner N 1999 Diffusion characteristics of calcium alginate gels *Biotechnol. Bioeng.* **65** 605–10
[29] Mehmetoğlu Ü, Ateş S and Berber R 1996 Oxygen diffusivity in calcium alginate gel beads containing Gluconobacter suboxydans *Artif. Cells Blood Substit. Immobil. Biotechnol.* **24** 91–106
[30] Cheema U, Rong Z, Kirresh O, MacRobert A J, Vadgama P and Brown R A 2012 Oxygen diffusion through collagen scaffolds at defined densities: implications for cell survival in tissue models *J. Tissue Eng. Regen Med.* **6** 77–84
[31] Tirella A, Orsini A, Vozzi G and Ahluwalia A 2009 A phase diagram for microfabrication of geometrically controlled hydrogel scaffolds *Biofabrication* **1** 45002
[32] Matyash M, Despang F, Ikonomidou C and Gelinsky M 2014 Swelling and mechanical properties of alginate hydrogels with respect to promotion of neural growth *Tissue Eng Part C Methods* **20** 401–11
[33] Tabriz A G, Hermida M A, Leslie N R and Shu W 2015 Three-dimensional bioprinting of complex cell laden alginate hydrogel structures *Biofabrication* **7** 45012
[34] Senbanjo L T and Chellaiah M A 2017 CD44: a multifunctional cell surface adhesion receptor is a regulator of progression and metastasis of cancer cells *Front Cell Dev. Biol.* **5** 18
[35] Ioannou M *et al* 2015 HIF-1α in colorectal carcinoma: review of the literature *J BUON* **20** 680–9
[36] Wielenga V J M *et al* 1998 CD44 splice variants as prognostic markers in colorectal cancer *Scand J. Gastroenterol.* **33** 82–7
[37] Bachtiary B *et al* 2003 Overexpression of hypoxia-inducible factor 1alpha indicates diminished response to radiotherapy and unfavorable prognosis in patients receiving radical radiotherapy for cervical cancer *Clin. Cancer Res.* **9** 2234–40
[38] Bos R, van der Groep P, Greijer AE, Shvarts A, Meijer S, Pinedo HM, Semenza GL, van Diest PJ, van der Wall E *et al* 2003 Levels of hypoxia-inducible factor-1α independently predict prognosis in patients with lymph node negative breast carcinoma *Cancer.* **97** 1573–81
[39] Kunz-Schughart L A, Kreutz M and Knuechel R 1998 Multicellular spheroids: a three-dimensional *in vitro* culture system to study tumour biology *Int. J. Exp. Pathol.* **79** 1–23
[40] Chwalek K, Bray L J and Werner C 2014 Tissue-engineered 3D tumor angiogenesis models: potential technologies for anti-cancer drug discovery *Adv. Drug. Deliv. Rev.* **79–80** 30–9
[41] Tian X, Wang W, Zhang Q, Zhao L, Wei J, Xing H, Song Y, Wang S, Ma D, Meng L, Chen G *et al* 2010 Hypoxia-inducible factor-1α enhances the malignant phenotype of multicellular spheroid HeLa cells *in vitro Oncol. Lett.* **1** 893–7
[42] Fang Y and Eglen R M 2017 Three-dimensional cell cultures in drug discovery and development *SLAS Discov. Adv. life Sci. R D* **22** 456–72
[43] Mueller-Klieser W 1997 Three-dimensional cell cultures: from molecular mechanisms to clinical applications *Am. J. Physiol.* **273** C1109–23
[44] Minchinton A I and Tannock I F 2006 Drug penetration in solid tumours *Nat. Rev. Cancer* **6** 583–92
[45] Nyga A, Cheema U and Loizidou M 2011 3D tumour models: novel *in vitro* approaches to cancer studies *J. Cell Commun. Signal* **5** 239–48
[46] Del Nero P, Lane M, Verbridge S S, Kwee B, Kermani P, Hempstead B, Stroock A, Fischbach C *et al* 2015 3D culture broadly regulates tumor cell hypoxia response and angiogenesis via pro-inflammatory pathways *Biomaterials* **55** 110–8
[47] Johnson L A *et al* 2013 Matrix stiffness corresponding to strictured bowel induces a fibrogenic response in human colonic fibroblasts *Inflamm Bowel Dis.* **19** 891–903
[48] Basakran N S 2015 CD44 as a potential diagnostic tumor marker *Saudi. Med. J.* **36** 273–9
[49] Cao D, Hou M, Guan Y, Jiang M, Yang Y and Gou H 2009 Expression of HIF-1alpha and VEGF in colorectal cancer: association with clinical outcomes and prognostic implications *BMC Cancer* **9** 432